An overview of assessment tools for determination of Magnesium implant degradation *in vivo*

Hafiz Wajahat Hassan[a], Valeria Grasso[b], Olga Korostynska[a], Haroon Khan[a], Jithin Jose[b], Peyman Mirtaheri[a,*]

[a] *Oslo Metropolitan University, Faculty of Technology, Art and Design, Department of Mechanical, Electronic and Chemical Engineering, Oslo, Norway*
[b] *FUJIFILM VisualSonics, Amsterdam, The Netherlands*

Abstract

Medical implants made of biodegradable materials are advantageous for short-term applications as fracture fixation and mechanical support during bone healing. After completing the healing process, the implant biodegrades without any long-term side effects nor any need for surgical removal.

In particular, Magnesium (Mg) implants, while degrading, can cause physiological changes in the tissues surrounding the implant. The evaluation of structural remodeling is relevant, however, the functional assessment is crucial to provide information about physiological changes in tissues, which can be applied as an early marker during the healing process. Hence, non-invasive monitoring of structural and functional changes in the surrounding tissues during the healing process is essential, and the need for new assessing methods is emerging.

This paper provides an assessment of Mg based implants, and an extensive review

⋆Word Count: 5298.

⋆⋆**Abbreviations:** BLL, Beer Lambert Law; CcO, cytochrome-c-oxidase; CtOx, cytochrome oxidase; CT, Computed Tomography; DPF, Differential Pathlength Factor; DX, Digital Radiography; FPCT, EDAX, energy dispersive X-ray analysis; Flat Panel Computed Tomography; ICG, Indocyanine Green; IV, intravascular; MBLL, Modified Beer Lambert law; MC, Monte Carlo Simulation; MDCT, Multi-Detector Computed Tomography; Mg, Magnesium; MRI, Magnetic Resonance Imaging; MRS, Magnetic Resonance Spectroscopy; NIRS: Near Infrared Spectroscopy; PAI, Photoacoustic Imaging; PET, Positron Emission Tomography; PLS, Partial Least Square; RTE, Radiative Transfer Equation; SRμCT, Synchrotron Radiation-based micro-Computed Tomography; StO2,saturated oxygen; THb, total tissue hemoglobin; THI, total hemoglobin index; USPA, Ultrasound and Photoacoustic; X- ray, Radiography.

*Corresponding author
Email address: peymanm@oslomet.no (Peyman Mirtaheri)

of the literature is presented with the focus on the imaging techniques used to monitor the biodegradation of Mg implants. The potential of a hybrid analysis, including Near-Infrared Spectroscopy (NIRS) and Photoacoustic Imaging (PAI) technology, is further discussed. A hybrid solution may play a significant role in monitoring implants and have several advantages for monitoring tissue oxygenation in addition to tissue's acidity, which is directly connected to the Mg implants degradation process. Such a hybrid assessment system can be a simple, ambulant, and less costly technology with the potential for clinically monitoring of Mg implants at site.
Keywords: Biodegradable implants, Mg implants, Imaging technique for Mg implants, Near-Infrared Spectroscopy (NIRS), Photoacoustic Imaging, Physiological Parameters

1. Introduction

Each year, millions of patients are treated for bone injuries from accidents and athletic activities, due to bone and osteoporotic fractures [1, 2]. In reconstructive surgery, the fractured bone may need internal fixation. To maintain stability during the healing process, the fixation is managed by the metal implants. Optimally, the metal implants should often be removed when the bone is healed. Thus it may cause complications such as impaired wound healing, infections, postoperative bleeding, and tissue and nerve damage [3]. Furthermore, metal implants have additional disadvantages, such as implant debris, allergic reaction, delayed union and non-union, metal sensitization, and mutagenicity [4]. Lately, several advancements in the field of biomaterial have resulted in new biodegradable implants based on ceramics, glass ceramics, polymers, composites, and metal alloys [5]. Upon implantation, physiological parameters such as pH, temperature, ionic content, and the presence of proteins change due to the formation and composition of the degradation layer [5].

The use of Mg alloys as degradable and biocompatible material is described as an innovative research field [6]. Biodegradable alloys used as stents and screws that

are based on Iron (Fe) and Magnesium (Mg) are expected to degrade. The existing imaging techniques used for monitoring Mg implants $in\ vivo$ are Magnetic Resonance Imaging and Spectroscopy (MRI, MRS), Computed Tomography (CT), Positron Emission Tomography (PET), Ultrasound and Photoacoustic (USPA) imaging, and hybrid technologies (e.g., PET-CT, and PET-MRI). These techniques provide pathological and morphological data [7].

Conceptually imaging techniques can be divided into two approaches: anatomical/structural and functional. The structural imaging approaches are specifically designed to visualize and analyze anatomical properties. To visualize the damage and abnormalities in the bones, geometrical structural features such as length, thickness and volume can be achieved. On the other hand, functional imaging provides information about metabolism, regional chemical, blood flow, and absorption rates [8, 9, 10, 11, 12, 13]. Through a combination of structural and functional imaging, it is possible to fully evaluate the degradation process.

Near-Infrared Spectroscopy (NIRS) and Photoacoustic Imaging (PAI) are considered as imaging techniques that are commonly used in soft tissues for accessing the blood and tissue-related functional properties. As blood maintains the communication between the external environment and cells of different body parts, the measurements in the tissue bed contain information about the interface between implants and tissue. Current NIRS techniques enable measuring the oxygen (O_2) delivery, pH, and blood flow in the tissue providing a local assessment of metabolic and respiratory status.

The main objective of this study is to review the Mg implants and their biodegradability *in vivo*, along with related imaging techniques. Further NIRS and PAI are elaborated with their advantages, as accessible, mobile in a hybrid instrument.

2. Biodegradable Mg implants

Magnesium degrades completely in a biological environment and it is an essential non-toxic element. Due to bioresorption, stimulated bone growth, and chronic inflammatory reactions, biodegradable implants are given much attention. In many

metabolic mechanisms, Mg^{2+} is actively involved as it has a significant presence in the human body (20-26g in an adult human, distributed in bones, muscles, and soft tissues) [14]. After implantation, the surrounding tissues and metabolic system can absorb or excrete the corrosion products of Mg alloy, produced by the electrical reaction to avoid postoperative surgery because it is easily converted to soluble and non-toxic oxide[15]. The Mg alloys have stimulating effects on osteoconduction and osseointegration [16]. Beside this, degradation rate and strength are important factors to consider the biocompatibility of the materials.

The biological effects and possible gas formation for biodegradable Mg implants are extensively described by Kim et al. based on *in vivo* histological analysis and gas volume [17]. The maximum gas volumes are $421.27 \pm 143.47 mm^3$ that are formed within 5 and 7 days after implantation. However, the volume of the produced gas depends on the size of the implant and the related tissue. The main components of the produced gases are hydrogen (H_2), carbon monoxide (CO) and carbon dioxide (CO_2). The physiological changes occur around the implant when Mg implants degraded with moderate pH changes and gas formation [18].

The metabolic rate, tissue oxygenation, cell growth and division, wound healing, and regeneration process are highly dependent on local pH levels in tissue [19, 20]. Most biodegradable Mg alloys, and polymers are known to influence the pH of the surrounding tissue [21, 22]. It is believed that Mg degrades in the body as Mg^{2+} ions and it reacts with salts and ions to create a degradation layer. Mg degradation causes a formation of gas and hydroxide ions which further increase the local pH significantly. As a result an adverse impact on the local cell's functionality will occur [23].

Corrosion behavior of Mg in Hank's solution was studied with a pH range of 5.5 to 8.0 (bone fracture healing implant is likely to be exposed in this pH range) by monitoring the rate of hydrogen gas evolution[24]. The pH value can differ greatly in biomedical applications from those found in the laboratory because $in\ vivo$ conditions are extremely complex. It has been reported that upon implantation, pH value of body fluid may decrease to a value around 5.2, and then recover to 7.4 within weeks, but it also needs to be monitored by the optical techniques [25].

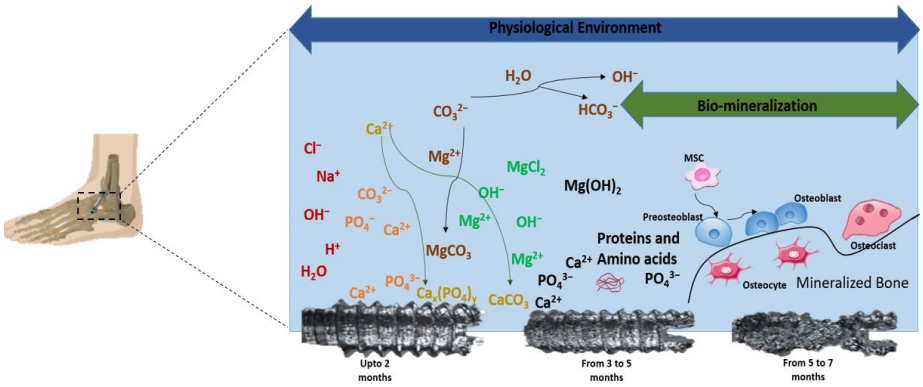

Figure 1: The Physiological interface of tissue/implant during biodegradation process

Mg and its alloys are suitable for fracture fixation because they possess the mechanical properties similar to human bones, highly biocompatible features, and can stimulate bone regeneration process [26]. The physiological processes involved during the Mg implant degradation is shown in Fig. 1. Mg implants interact with blood, and a degradation layer is formed by the reaction of electrostatic ions (Mg and salt ions) and water interaction. The cells, in turn, adjust the availability of these compounds during the process of degradation and metabolize Mg [18, 27]. The degradation products are supposed to adhere to the bulk material's interface and the newly formed tissue until the implant is thoroughly degraded and tissue remodeling occurs. The addition of organic and non-organic compounds may affect the degradation rate and physiological changes at the implant-tissue interface. When magnesium is in contact with extracellular fluid, it rapidly induces hydrogen gas, leading to subcutaneous bubbles. The process can delay the healing and even have toxication or wound dehiscence on the surrounding tissues [28, 29].

In general conditions in air, the Mg surface is covered by its oxides at room temperature, but any contact with moisture converts the oxide layer into hydroxide. In the vicinity of the implant surface, bacterial infection may result in an even more wider range of pH, from acidic to alkaline (4.0 to 9.0, respectively). The local biological micro-environmental changes in extracellular fluid, such as change in a pH, may influence cell metabolism, bone tissue development and mineralization.

3. Imaging techniques for Monitoring Mg implant

Investigating the Mg based implants, at a micro-and macro-structure level during the *in vivo* degradation process, is essential [30]. The degradation layer, biological environment, and the border between the degradation layer, consisting of several tens of micron, is enough to keep the implant in place. Thus, examining the structural properties of the degeneration interface requires imaging modalities equipped with high resolution. The golden standard CT and x-rays can achieve image resolutions of a few hundred microns, and therefore, cannot resolve the thickness of ~ 10 microns within the degradation layer [31].

Table 1: Existing imaging technologies that could be applied for Mg implants. [31, 32, 33, 34]

Comparative Analysis of different Imaging Techniques					
Imaging Technologies	**Nature of Signal**	**Spatial Resolution**	**Temporal Resolution**	**Key Advantages**	**Key Disadvantages**
NIRS	Oxy-,Deoxy-, and total- hemoglobin	Good ($\sim 2cm$)	Good ($ps-s$)	1.Metabolic information 2.Highly sensitive to variation and inexpensive	1. Limited structural information 2.Scattering and deep tissue issues
Ultrasound	Anatomical (Metabolic)	Excellent ($\sim 50-200\mu m$)	Low (s-min)	1.Non-invasive 2.Metabolic information 3.Dynamic, Non-ionizing radiation	1.Sensitive to air bubbles
X-ray	Metabolic	Good (1 mm)	Good (ms)	1.Low radiation dose 2.Metabolic information	1. May effect tissues and skin, when expose to higher radiation.
CT	Anatomical	Good (0.5 to 0.625 mm)	Good ($\sim 83-135ms$)	1.Widely available 3.Calcification detection	1. Radiation burden 2. Limited soft tissue contrast
Photoacoustic Tomography	Oxy-, Deoxy, and total hemoglobin	Excellent Spatial resolution depends on ultrasonic transducer ($\mu m-mm$)	Excellent (<100 μs)	1.Hybrid structural,molecular and functional	1. Relatively low temporial resolution
MRI/fMRI	Anatomical Blood oxygen Level-Dependent	Good ($\sim 3-6mm$)	Low ($\sim 1-3s$)	1. Structural Metabolic information 3. Excellent soft tissue contrast	1.Longer scan duration than CT 2.Extremely sensitive to movements 3. Heat issues
PET	Uptake of glucose metabolism using specific radionucleotides	Good ($\sim 1-2mm$)	Poor (s-min)	1.Metabolic information 2.Whole Body Imaging (WBI) 3.Infection and inflammation involvement	1.Involves ionizing radiation 2.Due to poor spatial resolution Combination with CT and MR
SRμCT	Structural	Excellent (μm)	Low	1.Crack segmentation 2.High flux and Spatial resolution 3.Structural information	1.Limited $in\ vivo$ trails possible 2.Limited access 3.Relatively low temporal resolution 4. Invasive

Fluorescence and X-ray diffraction techniques have been applied to investigate implants for examining the degradation kinetics and mechanical properties[32]. Further, it is also reported that the material microstructure and bone deformation has been assessed by high-resolution synchrotron tomography that can show highly structural details [35].

Further studies are required to understand Mg implants' artifacts compared to the classic orthopedic alloys. In 2014, Filly et al. verified that Mg based implants induce fewer artifacts in imaging modalities such as MRI, Digital Radiography (DX), Multi-Detector Computed Tomography (MDCT), and high-resolution Flat Panel CT (FPCT) compared to standard titanium and stainless steel [31, 36]. Mg alloys' mechanical properties improve by adding calcium and yttrium, which has been studied by resonant ultrasound spectroscopy and eco-pulse methods [33]. The method is mostly used to access the incorporation of Mg implants in bone tissue. Biodegradable Mg screws' potential was studied for application in Osteonecrosis of the Femoral Head (ONFH) patients to fix vascular bone graft. Both CT and X-ray imaging analysis were used for ONFH patients to measure the degradation rate and alteration in Mg screw shape [37].

Investigation of the image artifacts with MRI using Mg and titanium screw implants *in vitro* have shown that Mg artifacts have less severity compared to titanium [31].

Further, we need to emphasize that positron emission tomography (PET) quantifies bone perfusion and metabolism, which can be categorized as a functional imaging method. However, it can visualize the tissue around the implant with low resolution, and it involves an injection of radiotracers [38].

Table 1 shows available imaging technologies, which are capable of investigating the structural and functional degradation changes. In the case of imaging modalities such as MRI, the resolution depends on the type of instrumentation used. A summary of clinically reported imaging technologies to interrogate the Mg implants' degradation are also shown in Table 2.

Table 2: Imaging techniques that are clinically applied for monitoring implants. [37, 31, 33, 39, 40]

Imaging Technologies	Purpose	Reference
Ultrasound and Resonant Ultrasound Spectroscopy	To examine the mechanial and elastic properties of Mg alloys using eco pulse method	[33]
X-ray	To calculate the alteration in (coefficient of variation) shape and $in\ vivo$ degradation.	[37]
X-ray	Study of degradation of Mg, and Hydrogen gas formation to evaluate the biocompatibility.	[40]
MRI	Investigation of maximal artifacts reduction and image quality between two metallic implants (Mg and Titanium screws).	[31]
CT	Finding the $in\ vivo$ degradation rate of Mg screw and serum level of Mg, phosphorus (P) and calcium (Ca).	[37]
$SR\mu CT$	To study the degradation of a $Mg-2Ag$ pin in a cell culture medium.	[39]

4. NIR Spectroscopy

NIRS was first introduced in 1977 by Jöbsis as a non-invasive technique for measuring brain activities through the bone, skin, and muscles [41]. Since then, NIRS has been applied in numerous investigations and clinical applications. NIRS is an optical technique that is non-invasive and can continuously monitor regional tissue oxygenation as NIR light is strongly absorbed by hemoglobin. However, a spectrum within the range of 650 to 1100 nm regions depicts absorption information of oxygenated and deoxygenated hemoglobin in addition to hydration, proteins, collagen, cytochrome oxidase (CtOx), and fat [42]. Light in the NIR optical window can penetrate deeper (up to few centimeters) in biological tissues because of its weak absorbance ratio, especially from hemoglobin, water, proteins, and collagens in the tissue. NIR light above 950 nm is absorbed strongly by water, and below 650 nm, it is strongly absorbed by the hemoglobin and other proteins [43]. The absorption spectra of oxygenated and deoxygenated hemoglobin in term of optical coefficients

that are obtained from the Beer-Lambert Eq.(1) in NIR spectral range are shown in Fig. 2.

$$A = \log(I_o / I) = \epsilon \times [hemoglobin] \times L \tag{1}$$

Where, A is the measured absorbance, I_o is the intensity of incident light, I is the intensity of transmitted light, ϵ is the molar extinction coefficient, and L is the path length. ϵ is a measure of how strongly hemoglobin absorbs the light at a particular wavelength.

In highly scattering medium such as muscle and bone tissue, the mean distance traveled by a photon is much greater than geometrical path length (L) defined as differential path length and its scaling factor is known as differential pathlength factor (DPF). Hence, the Modified Beer-Lambert Law (MBLL), incorporates as:

$$A(t,\lambda) = \log(I_o(t,\lambda) / I(t,\lambda)) = \epsilon(\lambda) \times [hemoglobin](t) \times L \times DPF(\lambda) + G(\lambda) \tag{2}$$

where G is the geometrical correction factor due to attenuation and it depends on the medium, geometry, and wavelength (λ). Light propagation in biological tissue depends on the combination of scattering, absorption, and reflection of photons, where the light beam angle determines the reflection. Scattering and absorption in tissue are wavelength dependent. Scattering decreases as the wavelength increases, and thereby facilitates NIR over the visible light.

The measured hemoglobin properties facilitate additional calculating information such as saturated oxygen (StO_2), total hemoglobin index (THI) and total tissue hemoglobin (THb). NIRS can be used to access microcirculation changes in local oxygenated and deoxygenated hemoglobin saturation [44]. Sublingual reflectance NIR spectrophotometry is used in cardiac surgery for deeper regional oxygenation. The method provides the microcirculatory oxygen redistribution [45]. NIRS has also been used for the prediction of metabolic rate, blood flow, and other quantities that can be measured non-invasively, which includes blood volume and redox state of

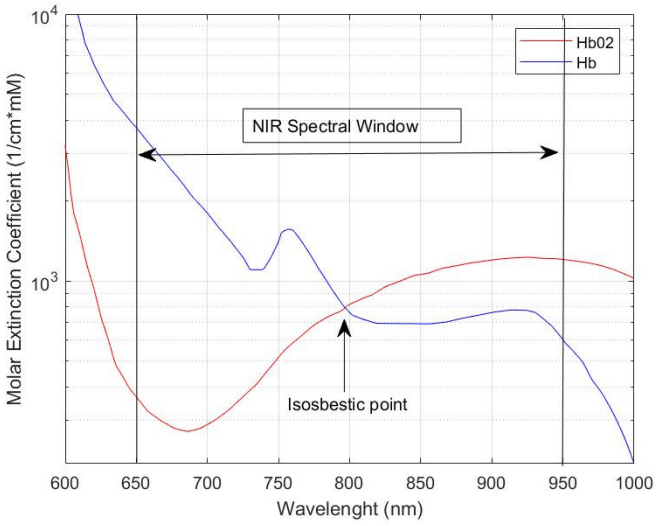

Figure 2: Molar extinction coefficient (ϵ) of oxygenated and deoxygenated hemoglobin

CuA Centre in cytochrome c oxidase [46].

For a dynamic environment with cost-effective solutions, NIRS is an appealing technique because of its non-invasive nature, ambulatory equipment, and inexpensive components. In the pre-operative phase, NIRS can assess the condition of individual organ or tissues. NIRS is an useful tool that can be applied in any organ, and the light beam can penetrate in the depth of several centimeters ($0.1 - 10cm$) depending on the application and tissue type [47, 48].

The NIR light propagating into the tissue is subject to multiple scattering, and the tissue's modeling of NIR light propagation has been an active field. Furthermore, such models provide insight into the experimental/clinical investigation. In the case of tissues with thickness > 1 cm, light diffusion under multiple disperse conditions has been accurately modeled using either Radiative Transfer Equation (RTE) or Monte Carlo (MC) Simulation [49]. The Beer-Lambert Law (BLL) is frequently used for tiny tissues samples, but its usefulness is often limited, especially for $in\ vivo$ imaging. NIR light propagation accurate modeling can be used in turbid media using MBLL. To quantify the variation in tissue chromophores concentration, MBLL

can be used for NIR spectroscopic data analysis. The MBLL approach empirically explains the optical attenuation in highly scattering media by using the Differential Pathlength Factor (DPF). The scaling factor (DPF) is dependent on wavelength, which indicates how much time the detected NIR light travelled [50]. DPF varies significantly between individuals, so incorrect values may result in significant measurement errors. In order to provide tissue type and tissue dimensions, Lambert-W based function modeling has been introduced and provides the tissue (of > 1cm thickness) properties parametrization that eventually leads to a generalized form of Beer-Lambert Law and provides improved results compare to MBLL [49].

4.1. Estimation of pH in tissue

The NIR spectra contain information about tissue oxygenation, blood flow, and the pH in the blood. A previous project at the optical/NIRS lab (Oslo Metropolitan University, Norway) has demonstrated that the spectroscopic method is feasible to indirectly measure both parameters using optical spectroscopical methods in the near-infrared range ($650-950nm$) [51]. In order to relate pH variations with spectral variations generated from the discrete reflectance measurement, within the wavelength range of 800 to 930 nm, a PLS (partial least square) multivariate regression model was used. Results has showed a significant NIR prediction of the pH in the blood. The relationship between the spectral data and measured pH values (ranging from $6.792-7.742$) was evaluated. The experimental dataset included NIR spectral data samples (26×1365) and 26 different response variables, the pH values measured from Blood Gas Analyser (BGA). The data set was pretreated through a third derivative algorithm to increase the spectral resolution and also find possible hidden information within the spectrum. As an example, Fig. 3a shows the plot of a series of spectra obtained by reflectance spectroscopy from arterial blood for 27 different blood pH values between 6.757 and 7.742. A Strong correlation was found between the area of interest from spectral range of $800-930nm$ and measured pH. For instance, Fig. 3b shows the plot for the reference vs. predicted pH values calculated by the PLS model with three principal components. The oxygen influence has

been examined more closely as hemoglobin changes induced by oxygen dominates spectral performances, even within this range of wavelengths. Furthermore, the PLS model suggests that it can perform well for these kinds of data sets. Table 3 provides a summary of PLS Validation. Blood serum tests with different pH values were performed for this experiment.

Table 3: PLS validation result[51]

	Elements	**pH-range**	**Factors**	**R2**	**RMSEP (pH Unit)**
PLS validation	25	6.792-7.742	3	0.906	0.089

5. Photoacoustic Imaging

PAI combines the advantages of ultrasound and optical methods. Although the technique was first introduced in 1880 by Alexander Graham Bell [52], only in the last few years the technique has been further exploited for biomedical imaging. A laser beam is shone into the tissue, while through its optical path, photons undergo multiple scattering within the tissue before being absorbed by the existing endogenous chromophores. Due to short-pulsed laser light, the optical energy absorbed by tissue is converted into heat, which induces a localized temperature increase ($< 0.1K$). Consequently, this causes a thermoelastic expansion that leads to the emission of ultrasonic pressure waves in the MHz range, which standard ultrasound transducers can detect [53]. Assuming that the speed of sound in biological tissue is homogenous ($\approx 1540 m/s$ for soft tissues surrounding a biodegradable bone implant) and identifying the time of arrival of acoustic signals, the respective optical absorption in the tissue can be reconstructed. An image of the ultrasound source signal is reconstructed by the regions of the highest optical absorption and with the exact spatial resolution as ultrasound images[54]. This combination of high spatial resolution and optical contrast makes PAI attractive for a wide range of studies involving micro-circulation abnormalities, and related conditions.

In summary, the PA image represents a map of the initial pressure distribution, which

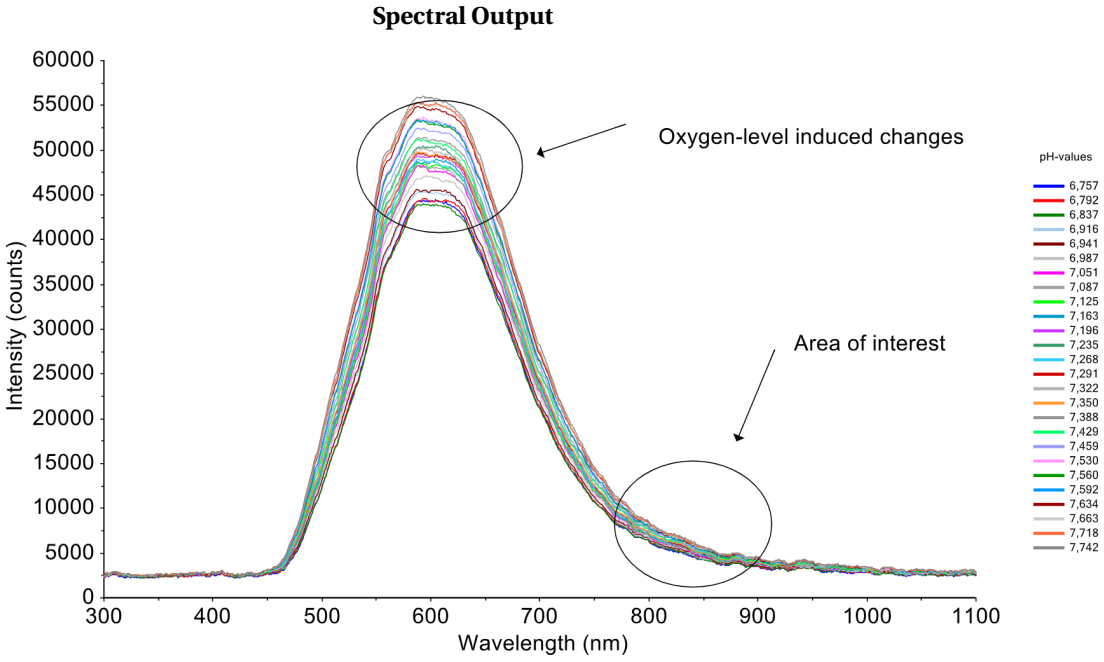

(a) NIR-Spectra of human blood

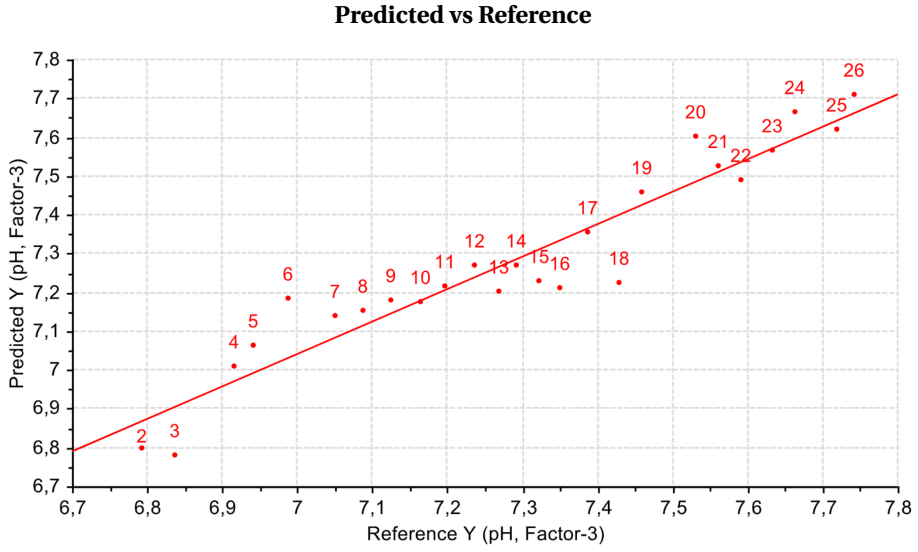

(b) Cross-validation

Figure 3: Spectra of human blood for a pH between (6.757 to 7.742) measured by continuous reflectance spectroscopy[51]; ; (a) optical spectra within the wavelength of 300-1100nm (b) Cross-validation plot of PLS predicted pH versus measured pH

is directly related to the absorbed light. Equation 3 describes the relationship between the detected photoacoustic (PA) waves with the fluence of the excitation light (Φ), the absorption coefficient of the irradiated tissue (μ_a), and the Gr$\ddot{u}$neisen coefficient (Γ).

$$PA(\lambda, z) = \mu_a(\lambda)\Phi(\lambda, z)\Gamma \tag{3}$$

where μ_a depends on the wavelength of the source light and Φ is depends on the depth at which the photons propagate at the respective wavelength (λ).

Since hemoglobin is the most prominent endogenous absorber in biological tissue, the NIR optical technologies have an excellent potential to investigate the tissue properties [55, 56]. Currently, most optical imaging technologies use lasers or light-emitting diodes (LED) as a probing source with the added advantage of being non-ionizing and the possibility of performing spectroscopic imaging. The techniques such as confocal microscopy (CM) and optical coherence tomography (OCT) enable resolution at the micron level at a limited imaging depth. Diffuse Optical tomography (DOT) is another commonly used imaging technique for the detection of molecular composition in tissue, and this approach enables deeper imaging ($< 100mm$) but with resolution in millimeters.

Conversely, as a hybrid modality, PAI offers a good compromise of visualizing tissue structures with micrometer resolution at deeper imaging depth. Since ultrasound scattering is two to three orders of magnitude weaker than optical scattering in biological tissues [53], PAI can provide a better resolution than optical imaging by detecting acoustic phonons instead of ballistic photons.

PAI has been used in a wide range of applications such as imaging tissue vasculature and angiogenesis, detection of tumor metastases, tissue oxygen saturation changes and therapy monitoring [57, 58, 59]. In addition to the endogenous absorbers, PAI is also used to detect the exogenous contrast agents. Indocyanine Green (ICG) is an exogenous molecular imaging agent widely used for various near-infrared fluorescence imaging technologies and ideally applied to PAI. Naturally, the use of contrast agents enhances the optical contrast increasing the PAI intensity. ICG is a clinically

approved dye detected using photoacoustic in several medical applications such as cardiology, liver function, perfusion studies, ophthalmic angiography, and cancer imaging [60, 61, 62, 63, 64]. Besides, the potential to image lymphatic drainage has been shown by performing ICG lymphography in patients with severe lymphedema [65].

Recently, PAI has also been used to monitor metallic implants and improve surgical procedures. Considering the high absorption coefficient in the NIR region of the metallic or composite materials, PAI is well suited to image coronary artery stents, needles, dental prosthesis, and brachytherapy seeds. Su et al. demonstrate the ability to visualize the stent during the surgery positioning procedure and post-surgery evaluations by using PAI [66]. Further, Lee et al. have conducted $Ex\ vivo$ PAI of a dental implant embedded in a porcine jawbone. In the study, they showed that PAI could provide information regarding the implant fixture, the bone anatomical features, and the thickness of the soft tissue above the bone [67].

Considering the current developments, PAI is a promising technology to follow the evolution of degradable Mg implants. The technology can image functional information by using the optical absorption of the oxygenated and deoxygenated hemoglobin. Indeed, continuous assessments of the oxygenation levels are essential to early identify issues due to the implantation procedure, and also as a follow up for the bio integration between the living tissues and the metallic implant. As an example, an inadequate and prolonged tissue oxygenation indicates irreversible tissue damage. However, if an inflammatory response occurs, there will be oxygenation variations and molecular alterations.

The excitation laser used for PAI is tunable in the NIR wavelength range; hence it is possible to illuminate the tissues sequentially at different wavelengths. Multi-wavelength photoacoustic imaging modality (also referred to as PAS) can be used to monitor other endogenous biomarkers such as melanin and lipids and the detection of the exogenous contrast agents [68, 69]. Since the tissue chromophores have distinct spectral signatures, multi-wavelength PAI can also be used to monitor the tissue spectral changes, which could be related to the disease conditions. For example, if physiological changes occur in the surrounding tissues due to the presence of

the metallic implant, spectral variations or additional absorbers could be detected using multi-spectral imaging approaches.

In the multispectral PAI, commonly linear regression algorithms are used to separate the different chromophores. These techniques have the limitation of being dependent on a priory knowledge of spectral signatures. Especially in presence of inflammatory response cases, this approach can be challenging due to the high variability and unpredictability of the spectral absorption of the tissue components. Indeed research efforts have been focused on developing automatic unmixing methods based on blind source separation algorithms that can be used to detect the prominent and less prominent absorbers in the tissue without any user interactions [70, 71].

Fig. 4 depicts the tissue-mimicking phantom set-up, which includes an Mg pin and a capillary tube filled with Indocyanine Green (ICG). Both samples were inserted into a chicken breast at a depth of $10mm$ from the surface, and carefully positioned with a spacing of $5mm$. The diameter of the Mg pin ($XHP-ZX00$ MgZnCa, BRI.TECH GmbH) was $1.6mm$, and the length was $8mm$. A capillary tube ($15\mu m$ inner diameter, $33\mu m$ outer diameter, and 16.5mm length) was filled with Indocyanine Green (ICG, PULSION Verwaltungs, GmbH), which was obtained at a concentration of $800\mu M$ by resuspending $25mg$ vial of ICG in sterile water. Multispectral PAI was performed with Vevo LAZR-X (FUJIFILM VisualSonics, Inc., Toronto, ON, Canada) with a linear array transducer of central frequency $21MHz$ ($MX250$). The details of the PAI set-up can be found elsewhere [71].

Fig. 4b, shows the spectral curves of ICG and Mg pin in the wavelength range of $680-970nm$. The spectral absorption graphs within the NIR range clearly show that Mg has a broad absorption spectrum, and the ICG has an absorption peak at around $880nm$. Fig. 4c shows the spectrally unmixed 3D PA image, where green and red voxels represent the spatial distribution of ICG and Mg, respectively. Since the chicken breast has limited absorption it is not detected from PAI, but visible in the ultrasound image and represented in grayscale.

When imaging in PA-Mode, from the experimental setup, the standard US transducer is combined with optical fibers fixed on the sides. This guarantees that the high-resolution US images are naturally registered to the laser-induced PA ultra-

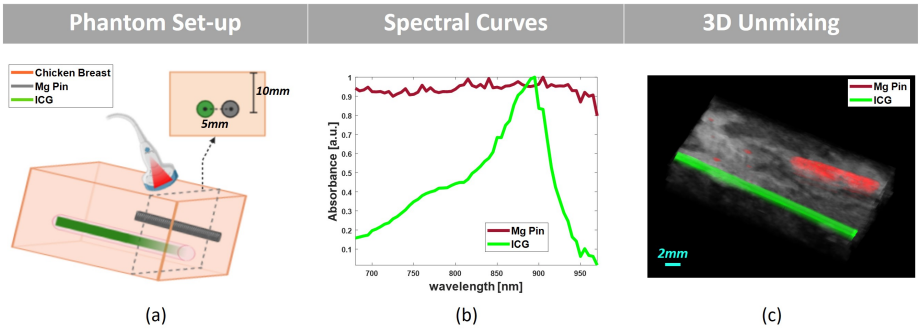

Figure 4: (a) Schematic of the tissue-mimicking phantom. (b) The PA absorbance spectral graph of ICG and Mg pin. (c) Spectrally unmixed 3D PA image.

sonic signals during spectral PAI acquisition. Therefore it is evident that the co-registration of USPA imaging demonstrates the feasibility of detecting anatomical, functional, and molecular information. Using a fully integrated USPA system allows the accurate detection of the metallic device in addition to the molecular information detectable from the implanted tissue environment. Ultrasound imaging can provide anatomical data such as the tissue structures, implant geometry, and tissue vascularity using the ultrasound Doppler functionality. Additionally, PAI can also provide partially functional information such as oxygen saturation, obtained by measuring the tissue absorption at $750nm$ and $850nm$ of the excitation light [72].

5.1. Hybrid imaging modality

During implant's follow up, it has become evident that monitoring implant performance and degradation with the existing imaging techniques is still a challenge: the contrast is weak for X-ray imaging. The use of conducting metal induces MR artifacts in addition to patient safety concerns. These scientific and technical issues constitute a significant barrier en route to broad clinical applications of biodegradable implants.

The imaging modalities are used primarily because of their respective ability to report structural and functional information. For choosing a reliable method, their

strengths and drawbacks to resolution, flexibility, tissue penetration depth, nature of radiation, absence or presence of the magnetic field, and the quantification of contrast are based on their principles. CT and PET are based on ionizing radiations, and continuous use may jeopardize patients' safety and health. Ionizing radiation from a PET and CT scan may also cause cellular response changes in subsequent radiation exposures [73]. Both CT and MRI provide details of the lesion site, morphology, size, and structural changes of neighboring tissues, and provide little insight into tumor physiology. Similarly, radiography has a limitation of providing necessary anatomical information for few tissue densities.

PET and fMRI provide functional and metabolic information, but PET involves radioactive material, and fMRI has limited temporal resolution affecting the hemodynamic response yielding biased estimation.

Ultrasound techniques commonly used in clinical research have numerous advantages, especially in surgery guidance, cardiology, and urology. However, to observe subtle anatomical details of the deep tissue, ultrasound techniques are not efficient. Functional imaging has an advantage over structural imaging to discriminate between living and damaged tissues. It can measure molecular and pathophysiological parameters, including blood flow, oxygenated and deoxygenated hemoglobin [74]. Future perspectives to combine the advantages from both $in\ vivo$ NIRS and PAI investigations would potentially enhance the detection of spectral changes that could occur in the soft tissues surrounding a biodegradable Mg based implant. Kole et al. [75] has proposed an intravascular (IV) setup that integrates IVPA-US and NIRS-IVUS to detect arterial lipid. The setup shows that combining two modalities enables accurate quantification and localization of lipid plaques in deep tissue. Hence, optical imaging solutions as NIRS and PAI may be among the modalities that can provide functional and structural data without exposure to ionizing radiation or high magnetic fields. These technologies can also be made as an ambulatory device that facilitates simpler examination procedures.

6. Discussion

Mg and its alloys degrade under physiological conditions, thus avoiding a second surgical intervention for implant removal after bone healing. The great challenge is to tailor the degradation with a suitable method for a biological environment. Fast or uncontrolled corrosion is associated with strong hydrogen, ion release, and severe pH changes, leading to a rapid loss of mechanical stability and undesirable biological reactions [76, 77]. Several $in\ vivo$ patient cases have reported supracondylar fractures, femoral fractures, or pseudarthrosis, that could successfully be treated with Mg implants [31]. The major and most common complication was the distinct hydrogen gas formation due to the Mg rapid degradation. The lack of knowledge on how to control the $in\ vivo$ degradation rate has probably caused the magnesium implant abandonment. These implants were replaced by corrosion resistant implants such as stainless steel for orthopedic surgeries. A study on biocompatibility and osteoblast cell culture has been done on Mg implants by Yun et al.[78], which consists of cell culture tests and corrosion test, environmental scanning electron microscope, and energy dispersive X-ray analysis (EDAX). Alkaline phosphatase staining study on bone tissue formation by Von Kossa also suggests the suitability of using Mg as a biodegradable implant material because it promotes bone mineralization [78].

NIRS has several advantages over other imaging techniques as portability, measuring changes in both oxygenated and deoxygenated hemoglobin, providing physiologically feasible non-invasively pH and blood flow measurements. Human tissue contains various substances whose spectra are well defined at NIR wavelengths, and their presence significantly attenuates the detected light. The concentration of the absorbers as water, bilirubin, and melanin remains constant over time. However, concetration of other absorbers as oxygenated and deoxygenated hemoglobin, and cytochrome-c-oxidase (CcO) changes with the state of oxygenation and metabolism of the cells. Blood flow and metabolic cell state are indicated by the tissue pH which is an important parameter in the Mg implant healing process. The pH can be calculated using NIR spectroscopy and multivariate methods with a significant sensitivity

[79]. A hybrid of NIR spectroscopy with PAI, would be a non-destructive method to biomechanical indentation as well as study the functional behavior in tissue[80]. Further, there is no involvement of any magnetic field or radio frequency (RF) pulses, which mitigate safety concerns[81]; although few studies assess the blood perfusion in bone[82]. NIRS [83] shows to assess knee joint ligament mechanical properties. Ligament and tendon biomechanical properties are estimated by NIRS, especially in tissue failure related parameters, which could be a potential advantage in monitoring Mg implant.

The early changes in tissue spectral signatures after the Mg implant, can also be monitored by a hybrid device with multi-spectral PAI and eventually detect the tissue inflammatory response. One of the challenges is to know changes in theoretical absorption spectra (such as oxygenated and deoxygenated hemoglobin spectra) in the presence of a biodegradable implant, which is interacting with the living tissue. The combination of NIRS and PAI enables the assessment of complementary information. In particular, local measurements using NIRS can be used as a priori information to unmix spectral PA imaging (spatial information from PA unmixed map combined to local NIRS specific). In addition to oxygenated and deoxygenated hemoglobin and other detected tissue components from PAI, and pH measurements from NIRS can be an indicator of the physiological conditions in the surrounded tissue around the implant. This is particularly relevant to monitor early inflammatory states and evaluate the implant's success in the long-term period. Furthermore, changes in scattering properties measured by NIRS can be combined with molecular assessments obtained by PAI and predict the implant's state.

Considering the strengths of the hybrid imaging modality, PAI can non-invasively and longitudinally monitor the Mg implant degradation and tissue regeneration in the clinical practice. Another promising prospect is to combine PAI with NIR fluorescent probe measurements. This approach can help to detect specific agents for monitor Mg implant degradation level, tissue regeneration, and inflammatory condition with enhanced specificity.

7. Conclusions

During the degradation process of Mg based implants, tissue pH and oxygenation levels change. Standard imaging techniques have not successfully examined the degradation layer and physiological changes around the implant non-invasively. NIRS can provide insight into the tissue blood flow, oxygenation level, and metabolism. However, the method lacks the spatial resolution to make a good image at the tissue-implant interface. PAI can provide structural information through ultrasound feasibility. A combination of NIRS and PAI has the potential to provide non-destructive and non-invasive methods to measure different tissue parameters in the human body.

Acknowledgments and funding

This publication is part of a project "Promoting patient safety by a novel combination of imaging technologies for biodegradable magnesium implants, MgSafe" that has received funding from the European Union's Horizon 2020 research and innovation program under the Marie Skłodowska-Curie grant agreement No 811226.

Disclosures

The authors declare that there are no conflicts of interest related to this article.

Ethical Approval

Ethics approval was not required for this study.

References

[1] W. R. Walsh, M. H. Pelletier, N. Bertollo, V. Lovric, T. Wang, P. Morberg, W. C. H. Parr, D. Bergadano, Bone ongrowth and mechanical fixation of implants in cortical and cancellous bone, Journal of Orthopaedic Surgery and Research 15 (1) (2020) 1–10. doi:10.21203/rs.3.rs-15923/v2.

[2] W. H. Organization, WHO scientific group on the assessment of osteoporosis at primary health care level, in: Summary meeting report, Vol. 5, 2004, pp. 5–7.

[3] R. Brown, E. Wheelwright, J. Chalmers, Removal of metal implants after fracture surgery–indications and complications., Journal of the Royal College of Surgeons of Edinburgh 38 (2) (1993) 96–100.

[4] M. Caicedo, L. Samelko, N. Hallab, Implant Material Bio-compatibility, Sensitivity, and Allergic Reactions, 2019. doi:10.1007/978-3-319-33037-2_29-1.

[5] M. Prakasam, J. Locs, K. Salma-Ancane, D. Loca, A. Largeteau, L. Berzina-Cimdina, Biodegradable materials and metallic implants—a review, Journal of Functional Biomaterials 8 (4) (2017) 44. doi:10.3390/jfb8040044.

[6] F. Feyerabend, H.-P. Wendel, B. Mihailova, S. Heidrich, N. A. Agha, U. Bismayer, R. Willumeit-Römer, Blood compatibility of magnesium and its alloys, Acta Biomaterialia 25 (2015) 384–394. doi:10.1016/j.actbio.2015.07.029.

[7] Z. Sun, K. Ng, N. Ramli, Biomedical imaging research: a fast-emerging area for interdisciplinary collaboration, Biomedical Imaging and Intervention Journal 7 (3) (2011). doi:10.2349/biij.7.3.e21.

[8] G. V. Hirsch, C. M. Bauer, L. B. Merabet, Using structural and functional brain imaging to uncover how the brain adapts to blindness, Annals of Neuroscience and Psychology 2 (2015). doi:10.7243/2055-3447-2-7.

[9] S. S. Keller, N. Roberts, Measurement of brain volume using mri: software, techniques, choices and prerequisites, Journal of Anthropological Sciences 87 (2009) 127–151.

[10] G. E. Alexander, J. R. Moeller, Application of the scaled subprofile model to functional imaging in neuropsychiatric disorders: a principal component approach to modeling brain function in disease, Human Brain Mapping 2 (1-2) (1994) 79–94. doi:10.1002/hbm.460020108.

[11] B. Crosson, A. Ford, K. M. McGregor, M. Meinzer, S. Cheshkov, X. Li, D. Walker-Batson, R. W. Briggs, Functional imaging and related techniques: an introduc-

tion for rehabilitation researchers, Journal of Rehabilitation Research and Development 47 (2) (2010) 27. doi:10.1682/jrrd.2010.02.0017.

[12] M. Min, P. Lin, G. Liney, M. Lee, D. Forstner, A. Fowler, L. Holloway, A review of the predictive role of functional imaging in patients with mucosal primary head and neck cancer treated with radiation therapy, Journal of Medical Imaging and Radiation Oncology 61 (1) (2017) 99–123. doi:10.1111/1754-9485.12496.

[13] A. Azari-Anderson, F. A. Chowdhry, Y. Ardeshirpour, N. S. Karamzadeh, E. G. Smith, V. Chernomordik, A. H. Gandjbakhche, Application of functional near-infrared spectroscopy in brain mapping, 2017, pp. 41 – 56.
URL http://dx.doi.org/10.1201/9781315373058

[14] J. W. Seo, T. J. Park, Magnesium metabolism, Electrolyte & blood pressure 6 (2) (2008) 86–95. doi:10.5049/EBP.2008.6.2.86.

[15] N.-E. L. Saris, E. Mervaala, H. Karppanen, J. A. Khawaja, A. Lewenstam, Magnesium: an update on physiological, clinical and analytical aspects, Clinica Chimica Acta 294 (1-2) (2000) 1–26. doi:10.1016/s0009-8981(99)00258-2.

[16] L. Mao, J. Chen, X. Zhang, M. Kwak, Y. Wu, R. Fan, L. Zhang, J. Pei, G. Yuan, C. Song, et al., A promising biodegradable magnesium alloy suitable for clinical vascular stent application, Scientific Reports 7 (2017) 46343. doi:10.1038/srep46343.

[17] Y.-K. Kim, K.-B. Lee, S.-Y. Kim, K. Bode, Y.-S. Jang, T.-Y. Kwon, M. H. Jeon, M.-H. Lee, Gas formation and biological effects of biodegradable magnesium in a preclinical and clinical observation, Science and Technology of Advanced Materials 19 (1) (2018) 324–335. doi:10.1080/14686996.2018.1451717.

[18] R. Willumeit-Römer, The interface between degradable Mg and tissue, JOM 71 (4) (2019) 1447–1455. doi:10.1007/s11837-019-03368-0.

[19] S. Schreml, R.-M. Szeimies, S. Karrer, J. Heinlin, M. Landthaler, P. Babilas, The impact of the pH value on skin integrity and cutaneous wound healing, Journal

of the European Academy of Dermatology and Venereology 24 (4) (2010) 373–378. doi:10.1111/j.1468-3083.2009.03413.x.

[20] Y. Shen, W. Liu, K. Lin, H. Pan, B. W. Darvell, S. Peng, C. Wen, L. Deng, W. W. Lu, J. Chang, Interfacial pH: a critical factor for osteoporotic bone regeneration, Langmuir 27 (6) (2011) 2701–2708. doi:10.1021/la104876w.

[21] F. Witte, N. Hort, C. Vogt, S. Cohen, K. U. Kainer, R. Willumeit, F. Feyerabend, Degradable biomaterials based on magnesium corrosion, Current Opinion in Solid State and Materials Science 12 (5-6) (2008) 63–72. doi:10.1016/j.cossms.2009.04.001.

[22] I. Bartsch, E. Willbold, B. Rosenhahn, F. Witte, Non-invasive pH determination adjacent to degradable biomaterials *in vivo*, Acta Biomaterialia 10 (1) (2014) 34–39. doi:10.1016/j.actbio.2013.08.047.

[23] I. Johnson, H. Liu, A study on factors affecting the degradation of magnesium and a magnesium-yttrium alloy for biomedical applications, PloS One 8 (6) (2013). doi:10.1371/journal.pone.0065603.

[24] W. Ng, K. Chiu, F. Cheng, Effect of pH on the *in vitro* corrosion rate of magnesium degradable implant material, Materials Science and Engineering: C 30 (6) (2010) 898–903. doi:10.1016/j.msec.2010.04.003.

[25] S. Virtanen, Biodegradable Mg and Mg alloys: Corrosion and biocompatibility, Materials Science and Engineering: B 176 (20) (2011) 1600–1608. doi:10.1016/j.mseb.2011.05.028.

[26] Q. Chen, G. A. Thouas, Metallic implant biomaterials, Materials Science and Engineering: R: Reports 87 (2015) 1–57. doi:10.1016/j.mser.2014.10.001.

[27] J. Gonzalez, R. Q. Hou, E. P. Nidadavolu, R. Willumeit-Römer, F. Feyerabend, Magnesium degradation under physiological conditions–best practice, Bioactive Materials 3 (2) (2018) 174–185. doi:10.1016/j.bioactmat.2018.01.003.

[28] G. Song, Control of biodegradation of biocompatable magnesium alloys, Corrosion Science 49 (4) (2007) 1696–1701. doi:10.1016/j.corsci.2007.01.001.

[29] G. Song, S. Song, A possible biodegradable magnesium implant material, Advanced Engineering Materials 9 (4) (2007) 298–302. doi:10.1002/adem.200600252.

[30] D. Chakkalakal, A. Mashoof, J. Novak, B. Strates, M. McGuire, Mineralization and pH relationships in healing skeletal defects grafted with demineralized bone matrix, Journal of Biomedical Materials Research 28 (12) (1994) 1439–1443. doi:10.1002/jbm.820281209.

[31] L. Sonnow, S. Könneker, P. M. Vogt, F. Wacker, C. von Falck, Biodegradable magnesium herbert screw–image quality and artifacts with radiography, CT and MRI, BMC Medical Imaging 17 (1) (2017) 16. doi:10.1186/s12880-017-0187-7.

[32] T. A. Grünewald, H. Rennhofer, B. Hesse, M. Burghammer, S. E. Stanzl-Tschegg, M. Cotte, J. F. Löffler, A.-M. Weinberg, H. C. Lichtenegger, Magnesium from bioresorbable implants: Distribution and impact on the nano-and mineral structure of bone, Biomaterials 76 (2016) 250–260. doi:10.1016/j.biomaterials.2015.10.054.

[33] A. Savin, N. Iftimie, R. Steigmann, G. Dobrescu, B. Istrate, C. Munteanu, Ultrasound methods for determining the influence of yttrium in Mg-0.5 Ca-xY, in: IOP Conference Series: Materials Science and Engineering, Vol. 572, IOP Publishing, 2019, p. 012017. doi:10.1088/1757-899x/572/1/012017.

[34] C. Martin, Contributions and complexities from the use of *in vivo* animal models to improve understanding of human neuroimaging signals, Frontiers in Neuroscience 8 (2014) 211. doi:10.3389/fnins.2014.00211.

[35] R. Willumeit-Römer, J. Moosmann, B. Zeller-Plumhoff, D. F. Wieland, D. Krüger, B. Wiese, A. Wennerberg, N. Peruzzi, S. Galli, F. Beckmann, et al., Visualization

of Implant failure by synchrotron tomography, in: TMS Annual Meeting & Exhibition, Springer, 2018, pp. 275–284. doi:10.1007/978-3-319-72526-0_25.

[36] W. R. Walsh, M. H. Pelletier, N. Bertollo, V. Lovric, T. Wang, P. Morberg, W. C. H. Parr, D. Bergadano, Bone ongrowth and mechanical fixation of implants in cortical and cancellous bone, Journal of Orthopaedic Surgery and Research 15 (1) (2020) 1–10.

[37] D. Zhao, S. Huang, F. Lu, B. Wang, L. Yang, L. Qin, K. Yang, Y. Li, W. Li, W. Wang, et al., Vascularized bone grafting fixed by biodegradable magnesium screw for treating osteonecrosis of the femoral head, Biomaterials 81 (2016) 84–92. doi:10.1016/j.biomaterials.2015.11.038.

[38] J. Czernin, N. Satyamurthy, C. Schiepers, Molecular mechanisms of bone 18F-NaF deposition, Journal of Nuclear Medicine 51 (12) (2010) 1826–1829. doi:10.2967/jnumed.110.077933.

[39] B. Zeller-Plumhoff, H. Helmholz, F. Feyerabend, T. Dose, F. Wilde, A. Hipp, F. Beckmann, R. Willumeit-Römer, J. U. Hammel, Quantitative characterization of degradation processes in situ by means of a bioreactor coupled flow chamber under physiological conditions using time-lapse SRμCT, Materials and Corrosion 69 (3) (2018) 298–306. doi:10.1002/maco.201709514.

[40] E. Aghion, G. Levy, S. Ovadia, *in vivo* behavior of biodegradable Mg–Nd–Y–Zr–Ca alloy, Journal of Materials Science: Materials in Medicine 23 (3) (2012) 805–812. doi:10.1007/s10856-011-4536-8.

[41] F. F. Jobsis, Noninvasive, infrared monitoring of cerebral and myocardial oxygen sufficiency and circulatory parameters, Science 198 (4323) (1977) 1264–1267. doi:10.1126/science.929199.

[42] F. Scholkmann, S. Kleiser, A. J. Metz, R. Zimmermann, J. M. Pavia, U. Wolf, M. Wolf, A review on continuous wave functional near-infrared spectroscopy and imaging instrumentation and methodology, Neuroimage 85 (2014) 6–27. doi:10.1016/j.neuroimage.2013.05.004.

[43] W. G. Zijlstra, A. Buursma, O. W. van Assendelft, Visible and near infrared absorption spectra of human and animal haemoglobin: determination and application, VSP, 2000.

[44] J. Vos, S. Ellermann, T. Scheeren, Journal of clinical monitoring and computing 2017/2018 end of year summary: monitoring—and provocation—of the microcirculation and tissue oxygenation, Journal of clinical monitoring and computing 33 (2) (2019) 201–209. doi:10.1007/s10877-019-00270-7.

[45] C. Ince, The microcirculation is the motor of sepsis, Critical Care 9 (4) (2005) S13–S19. doi:10.1186/cc3753.

[46] M. Banaji, A. Mallet, C. E. Elwell, P. Nicholls, C. E. Cooper, A model of brain circulation and metabolism: NIRS signal changes during physiological challenges, PLoS Computational Biology 4 (11) (2008). doi:10.1371/journal.pcbi.1000212.

[47] M. Lipcsey, N. C. Woinarski, R. Bellomo, Near infrared spectroscopy (NIRS) of the thenar eminence in anesthesia and intensive care, Annals of Intensive Care 2 (1) (2012) 1–9. doi:10.1186/2110-5820-2-11.

[48] A. Currà, R. Gasbarrone, A. Cardillo, C. Trompetto, F. Fattapposta, F. Pierelli, P. Missori, G. Bonifazi, S. Serranti, Near-infrared spectroscopy as a tool for *in vivo* analysis of human muscles, Scientific Reports 9 (1) (2019) 1–14. doi:10.1038/s41598-019-44896-8.

[49] M. Bhatt, K. R. Ayyalasomayajula, P. K. Yalavarthy, Generalized Beer–Lambert model for near-infrared light propagation in thick biological tissues, Journal of Biomedical Optics 21 (7) (2016) 076012–11. doi:10.1117/1.JBO.21.7.076012.

[50] D. A. Boas, T. Gaudette, G. Strangman, X. Cheng, J. J. Marota, J. B. Mandeville, The accuracy of near infrared spectroscopy and imaging during focal changes in cerebral hemodynamics, Neuroimage 13 (1) (2001) 76–90. doi:10.1006/nimg.2000.0674.

[51] H. Gunnlaugsdottir, Spectroscopic determination of pH in an arterial line from a heart-lung machine (2013).
URL http://urn.kb.se/resolve?urn=urn:nbn:se:kth:diva-121583

[52] N. B. Roozen, C. Glorieux, L. Liu, M. Rychtáriková, T. Van der Donck, A. Jacobs, Converting sunlight into audible sound by means of the photoacoustic effect: The heliophone, The Journal of the Acoustical Society of America 140 (3) (2016) 1697–1706. doi:10.1121/1.4962493.

[53] M. Xu, L. V. Wang, Photoacoustic imaging in biomedicine, Review of scientific instruments 77 (4) (2006) 041101. doi:10.1063/1.2195024.

[54] P. Beard, Biomedical photoacoustic imaging, Interface Focus 1 (4) (2011) 602–631. doi:0.1098/rsfs.2011.0028.

[55] Q. Pian, C. Wang, X. Chen, J. Liang, L. Zhao, G. Wang, X. Intes, Multimodal biomedical optical imaging review: towards comprehensive investigation of biological tissues, Current Molecular Imaging 3 (2) (2014) 72–87. doi:10.2174/22115552036661411172316 51.

[56] V. Ntziachristos, Going deeper than microscopy: the optical imaging frontier in biology, Nature Methods 7 (8) (2010) 603–614. doi:10.1038/nmeth.1483.

[57] S. Mallidi, K. Watanabe, D. Timerman, D. Schoenfeld, T. Hasan, Prediction of tumor recurrence and therapy monitoring using ultrasound-guided photoacoustic imaging, Theranostics 5 (3) (2015) 289. doi:10.7150/thno.10155.

[58] J. Jose, S. Manohar, R. G. Kolkman, W. Steenbergen, T. G. van Leeuwen, Imaging of tumor vasculature using twente photoacoustic systems, Journal of Biophotonics 2 (12) (2009) 701–717. doi:10.1002/jbio.200910025.

[59] Y. Zhu, T. Feng, Q. Cheng, X. Wang, S. Du, N. Sato, J. Yuan, M. Kuniyil Ajith Singh, Towards clinical translation of LED-Based photoacoustic imaging: A review, Sensors 20 (9) (2020) 2484. doi:10.3390/s20092484.

[60] M. Filippi, F. Garello, C. Pasquino, F. Arena, P. Giustetto, F. Antico, E. Terreno, Indocyanine green labeling for optical and photoacoustic imaging of mesenchymal stem cells after *in vivo* transplantation, Journal of Biophotonics 12 (5) (2019) e201800035. doi:10.1002/jbio.201800035.

[61] N. N. Nyström, L. C. Yip, J. J. Carson, T. J. Scholl, J. A. Ronald, Development of a human photoacoustic imaging reporter gene using the clinical dye indocyanine green, Radiology: Imaging Cancer 1 (2) (2019) e190035. doi:10.1148/rycan.2019190035.

[62] H. F. Zhang, K. Maslov, G. Stoica, L. V. Wang, Functional photoacoustic microscopy for high-resolution and noninvasive *in vivo* imaging, Nature biotechnology 24 (7) (2006) 848–851. doi:10.1038/nbt1220.

[63] I. Fox, A tricarbocyanine dye for continuous recording of dilution curves in whole blood independent of variations in blood oxygen saturation, Proc Mayo Clim 32 (1957) 478–484.

[64] J. Caesar, S. Shaldon, L. Chiandussi, L. Guevara, S. Sherlock, The use of indocyanine green in the measurement of hepatic blood flow and as a test of hepatic function, Clinical Science 21 (1961) 43–57.

[65] G. Giacalone, T. Yamamoto, F. Belva, A. Hayashi, Bedside 3d visualization of lymphatic vessels with a handheld multispectral optoacoustic tomography device, Journal of Clinical Medicine 9 (3) (2020) 815. doi:10.3390/jcm9030815.

[66] J. L.-S. Su, B. Wang, S. Y. Emelianov, Photoacoustic imaging of coronary artery stents, Optics Express 17 (22) (2009) 19894–19901. doi:10.1364/OE.17.019894.

[67] D. Lee, S. Park, W.-C. Noh, J.-S. Im, C. Kim, Photoacoustic imaging of dental implants in a porcine jawbone *ex vivo*, Optics Letters 42 (9) (2017) 1760–1763. doi:10.1364/OL.42.001760.

[68] Y. Cao, A. Kole, L. Lan, P. Wang, J. Hui, M. Sturek, J.-X. Cheng, Spectral analysis assisted photoacoustic imaging for lipid composition differentiation, Photoacoustics 7 (2017) 12–19. doi:10.1016/j.pacs.2017.05.002.

[69] E. Park, Y.-J. Lee, C. Lee, T. J. Eom, Effective photoacoustic absorption spectrum for collagen-based tissue imaging, Journal of Biomedical Optics 25 (5) (2020) 1–8. doi:10.1117/1.JBO.25.5.056002.

[70] S. Tzoumas, A. Nunes, I. Olefir, S. Stangl, P. Symvoulidis, S. Glasl, C. Bayer, G. Multhoff, V. Ntziachristos, Eigenspectra optoacoustic tomography achieves quantitative blood oxygenation imaging deep in tissues, Nature Communications 7 (2016) 1–10. doi:10.1038/ncomms12121.

[71] V. Grasso, J. Holthof, J. Jose, An automatic unmixing approach to detect tissue chromophores from multispectral photoacoustic imaging, Sensors 20 (11) (2020) 3235. doi:10.3390/s20113235.

[72] A. Needles, A. Heinmiller, J. Sun, C. Theodoropoulos, D. Bates, D. Hirson, M. Yin, F. S. Foster, Development and initial application of a fully integrated photoacoustic micro-ultrasound system, IEEE Transactions on Ultrasonics, Ferroelectrics, and Frequency control 60 (5) (2013) 888–897. doi:10.1109/TUFFC.2013.2646.

[73] K. Schnarr, T. F. Carter, D. Gillis, C. Webber, J. A. Lemon, I. Dayes, J. A. Dolling, K. Gulenchyn, D. R. Boreham, Biological response of positron emission tomography scan exposure and adaptive response in humans, Dose-Response 13 (4) (2015) 1559325815611904. doi:10.1177/1559325815611904.

[74] C. Avigo, A. Flori, P. Armanetti, N. Di Lascio, C. Kusmic, J. Jose, P. Losi, G. Soldani, F. Faita, L. Menichetti, Strategies for non-invasive imaging of polymeric biomaterial in vascular tissue engineering and regenerative medicine using ultrasound and photoacoustic techniques, Polymer International 65 (7) (2016) 734–740. doi:10.1002/pi.5113.

[75] A. Kole, Y. Cao, J. Hui, I. A. Bolad, M. Alloosh, J.-X. Cheng, M. Sturek, Comparative quantification of arterial lipid by intravascular photoacoustic-ultrasound imaging and near-infrared spectroscopy-intravascular ultrasound, Journal of Cardiovascular Translational Research 12 (3) (2019) 211–220. doi:10.1007/s12265-018-9849-2.

[76] R. Willumeit-Römer, W. Annelie, Special issue "Biodegradable magnesium as implant material, BioNanoMaterials 16 (1) (2015) 1–2. doi:10.1515/bnm-2015-0013.

[77] R. Willumeit, F. Feyerabend, N. Huber, Magnesium degradation as determined by artificial neural networks, Acta Biomaterialia 9 (10) (2013) 8722–8729. doi:10.1016/j.actbio.2013.02.042.

[78] Y. Yun, Z. Dong, D. Yang, M. J. Schulz, V. N. Shanov, S. Yarmolenko, Z. Xu, P. Kumta, C. Sfeir, Biodegradable Mg corrosion and osteoblast cell culture studies, Materials Science and Engineering: C 29 (6) (2009) 1814–1821. doi:10.1016/j.msec.2009.02.008.

[79] Y. Yang, O. O. Soyemi, M. R. Landry, B. R. Soller, Noninvasive $in\ vivo$ measurement of venous blood pH during exercise using near-infrared reflectance spectroscopy, Applied Spectroscopy 61 (2) (2007) 223–229. doi:10.1366/000370207779947657.

[80] M. Hoffmann, M. Lange, F. Meuche, T. Reuter, H. Plettenberg, G. Spahn, I. Ponomarev, Comparison of optical and biomechanical properties of native and artificial equine joint cartilage under load using nir spectroscopy, Biomedical Engineering/Biomedizinische Technik 57 (SI-1 Track-G) (2012) 1059–1061. doi:10.1515/bmt-2012-4099.

[81] J. Gervain, J. Mehler, J. F. Werker, C. A. Nelson, G. Csibra, S. Lloyd-Fox, M. Shukla, R. N. Aslin, Near-infrared spectroscopy: a report from the McDonnell infant methodology consortium, Developmental Cognitive Neuroscience 1 (1) (2011) 22–46. doi:10.1016/j.dcn.2010.07.004.

[82] T. Binzoni, S. Bianchi, J. Fasel, H. Bounameaux, E. Hiltbrand, D. Delpy, Human tibia bone marrow blood perfusion by non-invasive near infrared spectroscopy: a new tool for studies on microgravity, in: Life in Space for Life on Earth, Vol. 501, 2002, pp. 103–104.

[83] J. Torniainen, A. Ristaniemi, J. K. Sarin, S. Mikkonen, I. O. Afara, L. Stenroth, R. K. Korhonen, J. Töyräs, Near infrared spectroscopic evaluation of ligament and tendon biomechanical properties, Annals of Biomedical Engineering 47 (1) (2019) 213–222. doi:10.1007/s10439-018-02125-9.